processes

MDPI

Article

Experimental Study on the Vibration Reduction Performance of the Spindle Rotor of a Rubbing Machine Based on Aluminium Foam Material

Yao Yue, Haiqing Tian *, Dapeng Li, Fei Liu, Xin Wang, Xianguo Ren and Kai Zhao

College of Mechanical and Electrical Engineering, Inner Mongolia Agricultural University, Hohhot 010010, China
* Correspondence: hqtian@126.com

Abstract: Larger vibration and noise often exist in agricultural machinery due to the harsh working environment and high power. The rubbing machine is one of the indispensable pieces of equipment in the agriculture and livestock industry, and it is affected by the vibration of large constraints on its promotion and use. To reduce the vibration of the rubbing machine, the vibration characteristics of the spindle rotor were first analysed by modal simulation, thus determining the larger contributions to the spindle rotor vibration. Second, aluminium foam material was installed in the large deformation part of the spindle rotor. Its vibration reduction and energy absorption characteristics were used to optimise the vibration reduction design by increasing the damping. Third, a steel ball impact test was conducted to analyse the vibration characteristics of the optimised spindle rotor. The results show that the maximum impact accelerations were reduced by 28.4% and 64.75% in the axial and radial directions, respectively, and the impact energies were reduced by 67.3% and 90.65% in the axial and radial directions within 2 s of impact collision, respectively, indicating that the optimised spindle rotor damping increased significantly. In addition, the vibration reduction effect of the optimised rubbing machine was verified by a bench test. By measuring the change degree of the static component of the spindle rotor vibration, the axial, radial, and vertical vibrations of the spindle rotor were improved by 5.78%, 10.32%, and 23.96%, respectively. Therefore, optimising the spindle rotor with aluminium foam material can reduce the vibration generated during the impact of the material on the spindle rotor. The rubbing machine's vibration, damping, and energy absorption were also realised in real working conditions.

Keywords: aluminium foam material; attenuation vibration; vibration reduction and energy absorption; simulation test; impact test; damping ring

check for updates

Citation: Yue, Y.; Tian, H.; Li, D.; Liu, F.; Wang, X.; Ren, X.; Zhao, K. Experimental Study on the Vibration Reduction Performance of the Spindle Rotor of a Rubbing Machine Based on Aluminium Foam Material. *Processes* **2023**, *11*, 1038. https://doi.org/10.3390/pr11041038

Academic Editor: Ján Piteľ

Received: 24 February 2023
Revised: 24 March 2023
Accepted: 27 March 2023
Published: 29 March 2023

Copyright: © 2023 by the authors. Licensee MDPI, Basel, Switzerland. This article is an open access article distributed under the terms and conditions of the Creative Commons Attribution (CC BY) license (https://creativecommons.org/licenses/by/4.0/).

1. Introduction

Agricultural mechanisation is an inevitable trend in the development of modern agriculture, and agricultural machinery has made considerable achievements in quantity and efficiency. With the continuous improvement in the agricultural mechanisation level, higher requirements are put forwards for its accuracy, timeliness, and humanisation. However, large vibrations and noise often exist in agricultural machinery due to its harsh working environment and high power [1]. Large vibration and noise not only restrict the further improvement of agricultural mechanisation but also harm its operators' physical and mental health [2]. Stalk rubbing machines, as indispensable agricultural machinery in the process of stalk feeding, are widely used among farmers and herders. However, its further promotion is affected by the problem of large vibration and noise [3–5].

The design of vibration damping for agricultural machinery is mostly carried out by means of modal simulation analysis and resonance determination of several key components. This method is mostly used at the beginning of machine design, but for reasons such as manufacturing accuracy, this method does not easily dampen the machine after manufacturing or during use [6–8]. The rubbing machine uses the method of hitting and

rubbing to process the stalk. In the long run, the vibration gradually becomes larger. The way in which to reduce the vibration urgently needs to be solved. The stalk rubbing machine drives the rotor to rotate at high speed through the main shaft. Furthermore, the cutting knife on the rotor first cuts the stalk into small segments. After the impact and collision with the high-speed rotating hammer on the rotor and the tooth plate in the rubbing chamber, the stalk segments are broken into the stalk-like filamentous stalk, which is finally thrown out by the throwing blade. Therefore, the vibration of the entire rubbing process not only comes from the dynamic unbalance of the rotor rotating at high speed but also the nonuniformity of stalk feeding and the airflow disturbance in the rubbing room. For the vibration reduction of rubbing machines, previous research focused on the structure of rubbing machines and the law of the airflow field. The vibration reduction process is mostly only for specific components, and the process is complicated [9–18].

In this study, the finite element simulation was used to optimise the vibration reduction design of aluminium foam material installed on a rubbing machine rotor. The vibration reduction effect was verified by theoretical analysis and simulated stalk impact test. Aluminium foam is a microporous damping material with large pore size [19–22]. Due to its loose porous structure characteristics, it has the advantages of good impact energy absorption and high economic benefits. It is widely used in automobiles, railways, and other fields [23–25]. Specifically, Lu Xiaojun et al. studied the influence of the pore structure parameters of aluminium foam on the sound absorption coefficient, thus designing an impedance combined exhaust muffler with aluminium foam as a core tube [26]. A. G. Hanssen et al. investigated the three-point bending behaviour of a square beam filled with aluminium foam under quasi-static loading. The results showed that the foam filler significantly changed the local deformation pattern of the beam. Some scholars have also found that closed-cell aluminium foam can absorb much energy during quasitatic compression by undergoing a large amount of plastic deformation under low transfer stress [27]. Thus, aluminium foam is beneficial for developing energy absorbers, packaging, crash barriers, and other engineering applications that require efficient use of impact energy, in which lightweight design concepts are a key aspect [28,29]. All the above scholars found that aluminium foam materials have certain energy absorption and vibration reduction properties through test results. However, it is rarely used in agricultural machinery at present [30–32]. Taking the rubbing machine rotor as an example, this study explored the vibration reduction effect of aluminium foam material in a simulation test, providing theoretical support and a basis for its application in the vibration and noise reduction of rotary feed machinery.

2. Theoretical Basis

2.1. Modal Theory

In physical coordinates, a set of coupled second-order ordinary differential equations is often used to describe the motion of a multi-degree-of-freedom linear vibration system. The physical coordinates are transformed into modal coordinates using the vibration mode matrix; the ordinary differential equation can be transformed into a set of mutually independent motion equations, each of which has the same structure as a single degree-of-freedom vibration system. This analysis method is called modal analysis.

In modal coordinates, modal parameters (natural frequency, mode shape, modal stiffness, etc.) are usually used to describe the dynamic characteristics of the system. The modal parameters of the system can generally be obtained by analytical calculations or dynamic testing methods.

The differential equation of motion of a damped system with multiple degrees of freedom is then expressed as follows:

$$[M]\{\ddot{x}\} + [C]\{\dot{x}\} + [K]\{x\} = \{f\} \tag{1}$$

In the formula, $[M]$ is the mass matrix, $[C]$ is the damping matrix, $[K]$ is the stiffness matrix, $\{x\}$ is the response vector, and $\{f\}$ is the force vector.

Under the action of an external force, the motion equation in the form of the state vector of the system is

$$\begin{bmatrix} C & M \\ M & 0 \end{bmatrix} \begin{Bmatrix} \dot{x} \\ \ddot{x} \end{Bmatrix} + \begin{bmatrix} K & 0 \\ 0 & -M \end{bmatrix} \begin{Bmatrix} x \\ \dot{x} \end{Bmatrix} = \begin{Bmatrix} f \\ 0 \end{Bmatrix} \tag{2}$$

It is assumed that the external force acting on the system is simple and harmonic, that is,

$$\{f\} = \{F\} e^{i\omega t} \tag{3}$$

Then, the response of the physical coordinates and modal coordinates of the system is also simple and harmonic, namely,

$$\{x\} = \{X\}\, e^{i\omega t} \tag{4}$$

$$a_i = \begin{bmatrix} C & M \\ M & 0 \end{bmatrix} e^{i\omega t} \tag{5}$$

where $a_i = \begin{Bmatrix} \Psi_i \\ s_i \Psi_i \end{Bmatrix}^T \begin{bmatrix} C & M \\ M & 0 \end{bmatrix} \begin{Bmatrix} \Psi_i \\ s_i \Psi_i \end{Bmatrix}$.

The matrix expression of the frequency response function of the multi-degree-of-freedom damped system is derived by the state space method as follows:

$$[H(\omega)] = \sum_{i-1}^{n} \left(\frac{1}{a_i} \frac{\{\Psi_i\}\{\Psi_i\}^T}{i\omega - s_i} + \frac{1}{a_i^*} \frac{\{\Psi_i^*\}\{\Psi_i^*\}^T}{i\omega - s_i^*} \right) \tag{6}$$

Then, complex frequency is $s_i = -\frac{a_i}{b_i}$, $b_i = \begin{Bmatrix} \Psi_i \\ s_i \Psi_i \end{Bmatrix}^T \begin{bmatrix} K & 0 \\ 0 & -M \end{bmatrix} \begin{Bmatrix} \Psi_i \\ s_i \Psi_i \end{Bmatrix}$; $\{\Psi_i\}$ is a complex modal vector.

In addition, the relevant theories of the modal assurance criterion (MAC) are also used. The MAC matrix is the dot product of the vibration mode vectors and is a tool for evaluating the spatial correlation of the modal vectors. Its calculated variable values are between 0 and 1. Its expression is

$$\mathrm{MAC}_{ij} = \frac{\left(\phi_i^T \phi_j\right)^2}{\left(\phi_i^T \phi_i\right)\left(\phi_j^T \phi_j\right)} \tag{7}$$

where ϕ_i and ϕ_j are the i-th-and j-th-order vectors of the vibration mode matrix, respectively.

If ϕ_i and ϕ_j are estimates of the same vibration mode by the same parameter identification method, $i = j$. The two modal vectors can be converted to each other according to a certain scale factor, so the values should be close in theory; therefore, the value of the ratio MAC_{ij} should be close to 1. If different vibration modes are estimated, theoretically, the value is relatively low, and the ratio MAC_{ij} value should be close to 0.

2.2. Attenuated Vibration Theory

In free vibration, the mechanical energy of the vibration system remains constant, the vibration repeats indefinitely, and the amplitude remains constant. However, in the actual vibration system, due to damping, the mechanical energy of the vibration system gradually decreases; the amplitude gradually attenuates; and, finally, the bot tends to zero and stops vibrating. Such vibration is called attenuated vibration, and its vibration differential equation is as follows:

$$\ddot{x} + \frac{c}{m}\dot{x} + \frac{k}{m}x = 0 \tag{8}$$

Let $p_n^2 = \frac{k}{m}$, $2n = \frac{c}{m}$
where n is called the attenuation coefficient, and the unit is 1/s; p_n is the undamped vibration inherent in the system. The above equations can be written as follows:

$$\ddot{x} + 2n\dot{x} + p_n^2 x = 0 \tag{9}$$

The solution of the vibration differential equation is discussed in three cases of $n < p_n$, $n > p_n$, and $n = p_n$. According to the time domain diagram of this test, the solution of the vibration differential equation needs to be discussed in the case of $n < p_n$, that is, small damping.

From the theory of differential equations, the general solution of the equation is as follows:

$$x = e^{-nt}(C_1 cos p_d t + C_2 sin p_d t) \tag{10}$$

C_1 and C_2 are integral constants; when t = 0, $x = x_0$ and $\dot{x} = \dot{x}_0$, and thus we can obtain the following:

$$C_1 = x_0,\ C_2 = \frac{nx_0 + \dot{x}_0}{p_d}$$

Equation (10) can be written in the following form

$$x = Ae^{-nt}\sin(p_d t + \alpha) \tag{11}$$

The period of the function $\sin(p_d t + \alpha)$ is set as the period of the damped oscillation. Therefore, the period and frequency of the oscillation are

$$\tau = \frac{2\pi}{p_d} = \frac{2\pi}{\sqrt{1-\xi^2}p_n} \tag{12}$$

$$f = \frac{p_d}{2\pi} = \frac{\sqrt{1-\xi^2}p_n}{2\pi} \tag{13}$$

In the equation, $\xi = \frac{n}{p_n}$, where ξ is the ratio of the attenuation coefficient n to the natural frequency of the undamped free vibration of the system, which is called the damping ratio. When $n < p_n$, $\xi < 1$. According to Equations (12) and (13), damping can make the period of vibration longer and the frequency lower. Therefore, combined with the above equations, the image data obtained in the experiment can be processed and analysed to judge the vibration reduction effect of aluminium foam material.

3. Materials and Methods

3.1. Modal Test and Finite Element Simulation Analysis of Main Shaft Rotor of Rubbing Machine

3.1.1. Modal Test of Main Shaft Rotor of Rubbing Machine

The main shaft rotor is in the rubbing room. The rotor includes the main shaft, hob, hammer, hammer frame, throwing blade, and support plate, as shown in Figure 1. To determine the installation position of aluminium foam material, a modal analysis was carried out on the main shaft rotor of the rubbing machine. To further make the simulation results credible, a modal test was carried out on the main shaft rotor of the rubbing machine first, and the finite element simulation analysis results were corrected and adjusted according to the test results.

Because of the spindle rotor phase's small volume and light weight, the mode test was carried out by suspending the spindle rotor. To maintain the free state of the spindle rotor, rubber ropes were employed to suspend the spindle rotor. Avoiding the rubber rope and the part except for the suspension point contact is essential. This configuration is shown in Figure 2.

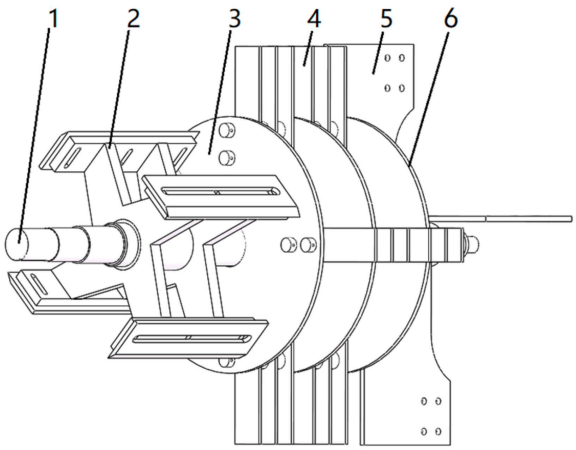

Figure 1. Three-dimensional model of the spindle rotor. (1) Spindle; (2) disc cutter; (3) hammer frame; (4) hammer; (5) throwing blade; (6) support plate.

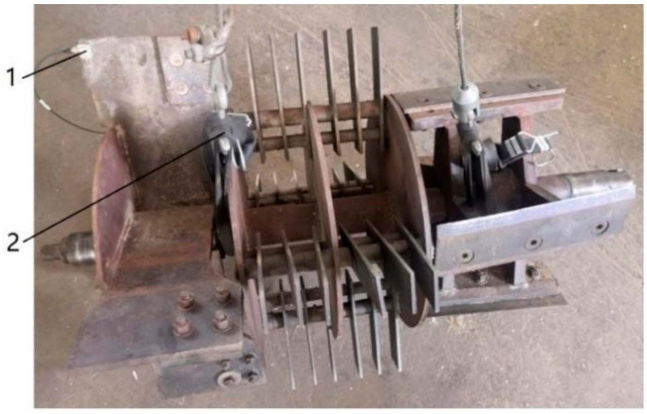

Figure 2. Modal test layout. (1) Suspension point; (2) sensor placement point.

Similarly, the three-dimensional wire diagram of the spindle rotor was drawn by CAD, and the modal test model of the spindle rotor was established. The main connection points, centre points, and boundary points of each component of the spindle rotor were selected as knocking measuring points. A total of 57 knocking measuring points were selected, and the three-axis vibration acceleration sensor was arranged at the end of the throwing blade of the spindle rotor, as shown in Figure 3.

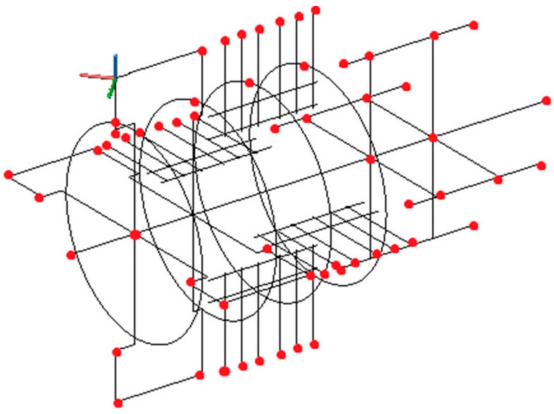

Figure 3. Test point of spindle rotor modal test diagram.

According to the actual working conditions of the spindle rotor, the line value was selected as 400 Hz, span as 400 Hz, and linear as the average mode. In the spindle rotor

modal test, three axes of each measuring point were struck, and each knock was repeated three times. The frequency response function of the excitation measuring point signal is shown in Figure 4. It is known that the rigid body modal frequency caused by suspension is far less than that of the first-order elastic mode, indicating that the support conditions of the test system do not influence the first-order elastic mode of the spindle rotor.

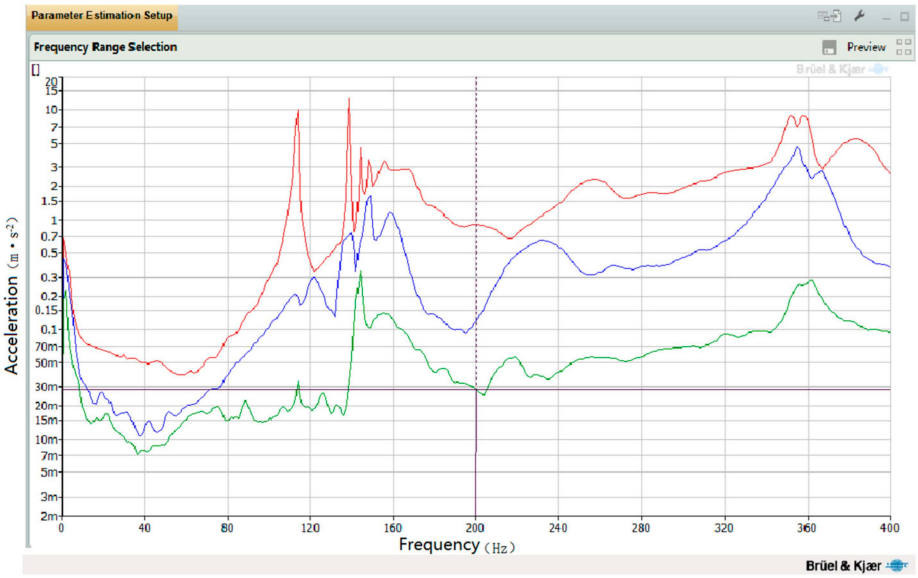

Figure 4. Spindle rotor frequency response function.

The PULSE Reflex module in PULSE software was used to analyse the data collected from the modal test of the spindle rotor, and the low-frequency band of 40~360 Hz was selected to extract the modal frequency band of each order. The test results are shown in Table 1.

Table 1. First 6 natural frequencies.

Order	Frequency/Hz	Damping/%
1	113.59	0.90
2	138.59	0.24
3	143.83	0.39
4	154.31	2.34
5	233.34	5.66
6	262.38	3.72

The correlation of the modal shapes of the spindle rotor was analysed, and the MAC matrix modal confidence criterion was obtained. Figure 5 shows that according to the MAC matrix modal confidence criterion, the MAC value of the same mode was 1, indicating that the theoretical modes were correlated. For the values other than the off-diagonal matrix, it is indicated that the independence of each order calculation mode was good, and the correlation was small, which indicates that the test effectively extracted the modal parameters of the structure. The modal test results of the spindle rotor had high credibility.

3.1.2. Finite Element Simulation Analysis of Rubbing Machine Spindle Rotor

The 3D model of the spindle rotor was established with Solidworks software and imported into the finite element software for modal simulation. The main material was structural steel in an unconstrained free state with a density of approximately 7.9 kg·m^{-3}. The connection mode of each part of the spindle was set to be welded, and the grid was divided, as shown in Figure 6.

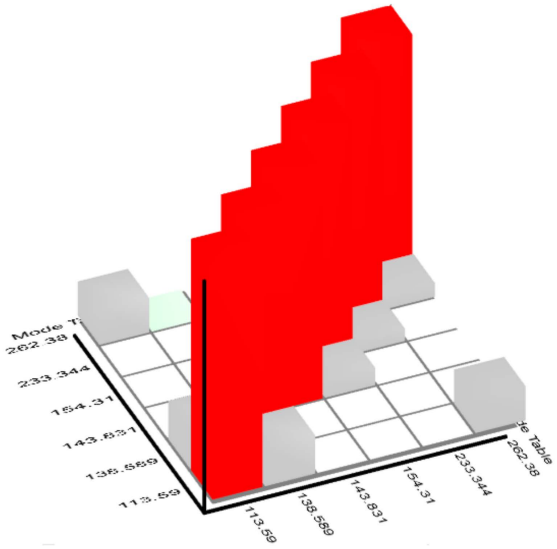

Figure 5. Spindle rotor mac matrix.

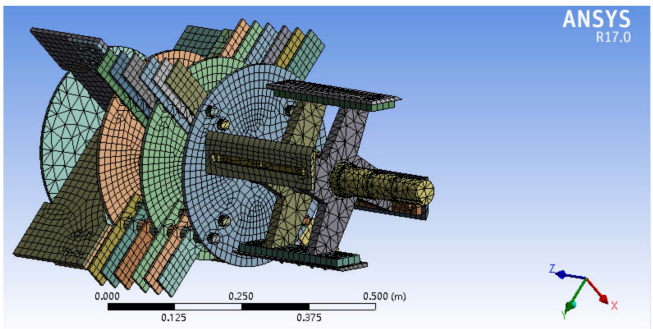

Figure 6. Spindle rotor simulation process.

Finite element modal simulation analysis was carried out in ANSYS Workbench finite element software. Because the first six modes obtained by simulation are rigid body modes and the model deformation is small, the 7th to 12th modes of the finite element simulation results were considered to correspond to the 1st to 6th modes of the modal test. The results of the finite element simulation test and modal test were compared and analysed, as shown in Table 2.

Table 2. Free modal test results and simulation results of the rotor of the rubbing machine.

Modal Test Results		Simulation Test Results		Error/%
Order	Frequency Hz	Order	Frequency/Hz	
1	113.59	7	116.77	2.8
2	138.59	8	139.03	0.3
3	143.83	9	144.54	0.5
4	154.31	10	156.04	1.1
5	233.34	11	223.53	4.2
6	262.38	12	285.22	8.7

Comparing and analysing the results of the modal test and finite element simulation, the error between the two matters for the corresponding order frequency was 8.7% at most and 0.3% at least. Hence, the results of the modal simulation test were consistent with the results of the modal test analysis. Parameters such as the spindle rotor's deformation and the spindle rotor's vibration mode can be obtained by the modal simulation test, as shown in Figure 7.

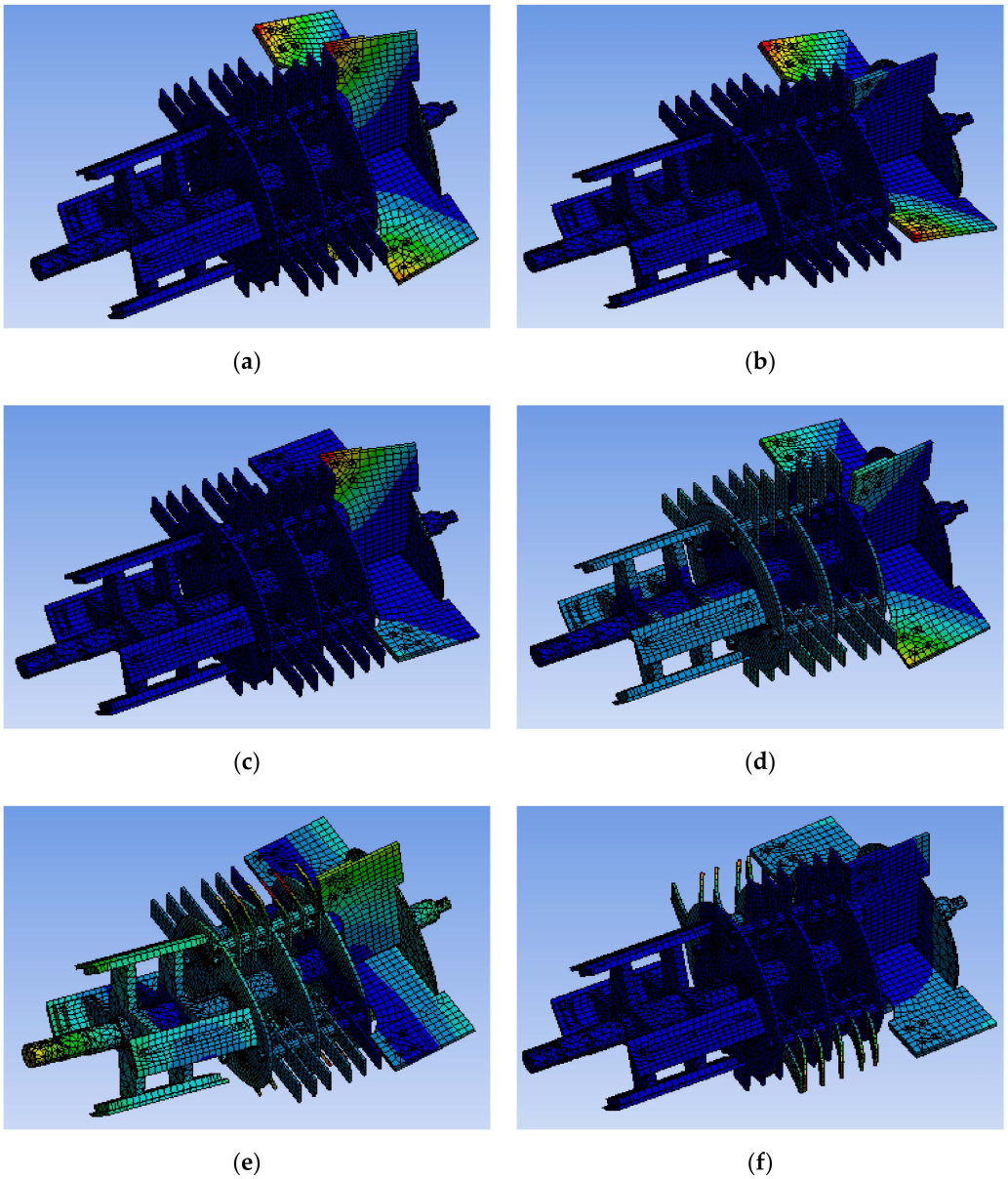

Figure 7. Mode shape diagram of each order. (**a**) The 7th order; (**b**) the 8th order; (**c**) the 9th order; (**d**) the 10th order; (**e**) the 11th order; (**f**) the 12th order.

As the primary power source of rotating machinery, the deformation of the spindle rotor will affect the vibration of the entire machine. According to the finite element simulation mode in Figure 7, the throwing blade deformation was obvious, the support plate connected with the throwing blade deformation was obvious, and the hob deformation was obvious. Therefore, in the optimisation design of vibration reduction, it is necessary to consider the optimisation of throwing blades, support plates, hobs, and other parts prone to deformation in order to improve the vibration of the spindle rotor.

3.2. Vibration Reduction Optimisation and Test Verification of the Main Shaft Rotor

According to preliminary tests and a literature review, when impact collision occurs between the stalk and rotor, the attenuation vibration of the throwing blade of the spindle rotor lasts longer. In continuous impact collision and throwing blade of the stalk, the vibration amplitude of the spindle rotor gradually strengthens, thus causing vibration of the entire stalk rubbing machine [33–41]. In addition, spindle rotation is the leading cause of stalk rubbing machine vibration. The finite element simulation results show that the

spindle rotor throwing blade, support plate, and hob deformation were large. At the same time, the vibration theory analysis shows that increasing the damping of the rotor can suppress the vibration and reduce the vibration amplitude. Therefore, when optimising the vibration reduction of the stalk rubbing machine, the method of increasing the damping of the rotor was adopted to optimise the vibration reduction. The aluminium foam material used in the optimisation design of rotor vibration reduction is shown in Figure 8.

Figure 8. Microcellular foam aluminium material.

On the basis of the results of vibration tests, vibration theory analysis, modal tests, and modal simulation, the vibration reduction optimisation design of the rotor's throwing blade, support plate, and hob shaft sleeve was carried out. In the optimisation design of vibration reduction, four pieces of 100 × 100 × 10 mm square aluminium foam materials were installed on the four pieces of the throwing blades and close to the shaft sleeve, and five pieces of triangular aluminium foam materials between each square aluminium foam sheet and adjacent blades. The aluminium foam material and throwing blade were fixed by glue bonding. The steel sheet and the throwing blade were welded to form extrusion pressure on the triangular aluminium foam material to prevent the aluminium foam material from falling off during the operation of the spindle rotor, as shown in Figure 9. In addition, damping rings made of aluminium foam were installed on the hob shaft bush and the support plate, as shown in Figures 10 and 11 [42]. Thus, the vibration reduction optimisation of the spindle rotor can be realised, and the vibration of the stalk rubbing machine can be solved.

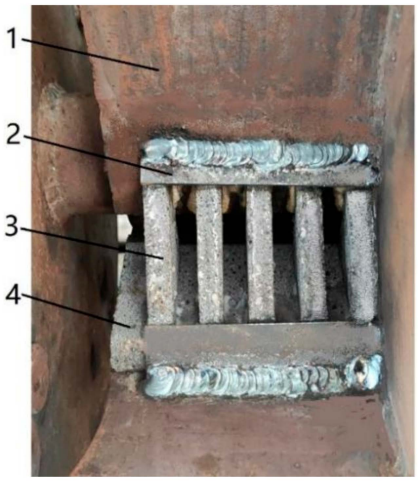

Figure 9. The installation position of the foamed aluminium material of the throwing blade. (1) Throwing blade; (2) steel plate; (3) triangular aluminium foam; (4) square aluminium foam.

Figure 10. Mounting position of the damping ring of the hob shaft sleeve. (1) Hob shaft sleeve; (2) damping ring.

Figure 11. Installation position of the support plate damping ring. (1) Support plate; (2) damping ring.

The principle of the steel ball impact vibration test is as follows. First, the steel ball has no initial velocity, and the potential energy of the steel ball is converted into kinetic energy to obtain the initial velocity. Then, it collides with the throwing blade of the spindle rotor to stimulate the spindle rotor to attenuate vibration under its damping effect. Consequently, the present study assumed that the motion between the ball and the throwing blade is a rigid collision. The same kinetic energy is obtained by making the falling height of the ball always before and after optimisation. Therefore, the vibration reduction effect of the vibration reduction optimisation of the spindle rotor can be analysed by comparing the mean value, mean square value, and variance of the vibration acceleration before and after the optimisation of the spindle rotor.

The steel ball impact vibration test was carried out in an environment without a large vibration source and electromagnetic interference. During the test, the steel ball (diameter of 10 mm, weight of approximately 4.11 g) at a fixed height (150 mm, 550 mm from the vertical direction of the excitation point) without an initial velocity impacted the free end of the throwing blade of the spindle rotor. The heights of 150 mm and 550 mm were selected as the near relative point and far point between the throwing blades, respectively, being representative. Before the impact vibration test of the steel ball, to avoid excessive contact between the rubber rope and the part except for the suspension point so that it was in a free state, the rubber rope was first used to hang the spindle rotor. This was to ensure that the vibration of the spindle rotor was only affected by the rotor itself and the environmental damping. On this basis, the steel ball impact vibration test system was built. The three-axis vibration acceleration sensor was arranged at the free end of the throwing blade and connected to the data acquisition card through the data transmission line to receive the vibration signal. The collected signal was analysed and stored by the PULSE software. The channels of the three-axis vibration acceleration sensor connected to the data

acquisition card corresponded to the axial and radial directions of the spindle rotor, as shown in Figure 12. In the steel ball impact vibration test, the line value was 1600 Hz, the span value was 400 Hz, and the sampling time was 4 s.

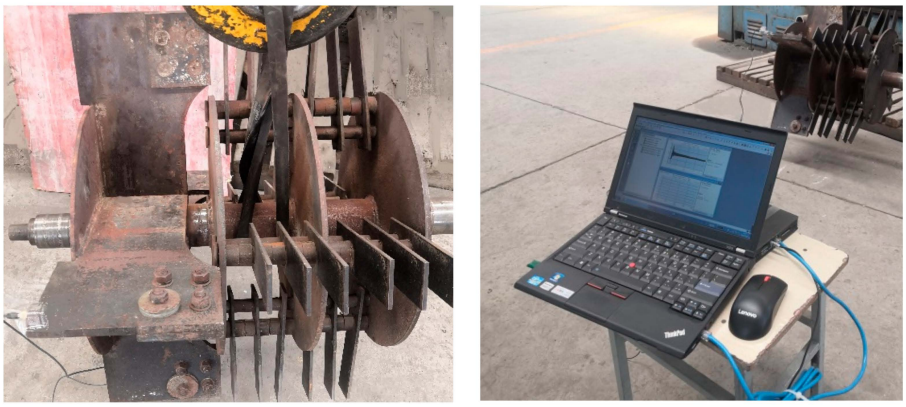

(**a**) (**b**)

Figure 12. Site of the steel ball impact vibration test. (**a**) Sensor placement; (**b**) steel ball impact vibration test system.

4. Results

The vibration signal was collected and analysed by the steel ball impact vibration test system, and the vibration law of the spindle rotor before and after vibration reduction optimisation was obtained. When the falling height of the steel ball was 550 mm, the axial vibration acceleration of the spindle rotor before and after vibration reduction optimisation was as shown in Figure 13a,b, respectively. Notably, the latter had a faster vibration attenuation and a smaller acceleration value.

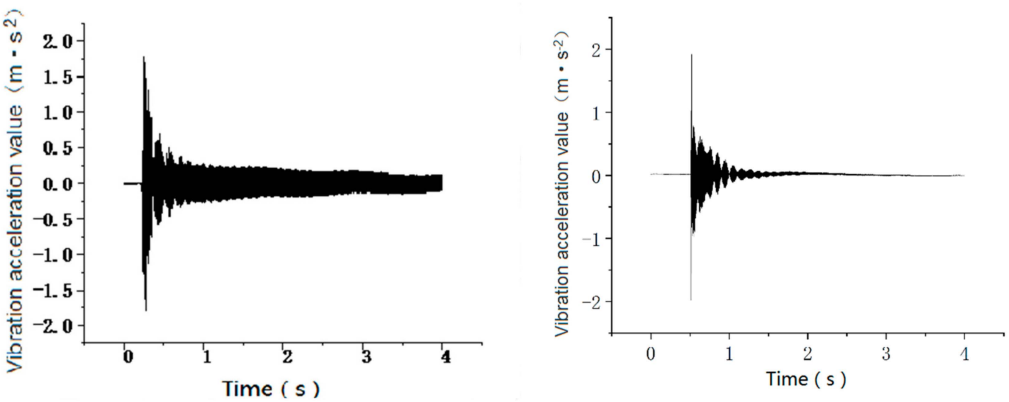

(**a**) (**b**)

Figure 13. Axial vibration acceleration before and after vibration reduction optimisation. (**a**) Axial vibration acceleration before optimisation; (**b**) axial vibration acceleration after optimisation.

Taking the maximum vibration acceleration as the initial time, the vibration variation law of the spindle rotor before and after the vibration reduction optimisation within 2 s after the initial time was studied. Through analysis, when the steel ball fell at 150 mm and 550 mm, the mean value, mean square value, and variance of the radial and axial vibration acceleration of the spindle rotor after vibration reduction optimisation were smaller than those before vibration reduction optimisation, as shown in Figure 14a,b. This indicates that the vibration system's static component, average energy, and fluctuation were reduced after vibration reduction optimisation. Given this, the vibration attenuation of the vibration system was faster, and the energy loss was more severe and tended to stabilise faster. In addition, by analysing the axial and radial vibration reduction effect of the optimised

spindle rotor, the mean values of the impact vibration acceleration of the steel ball were reduced by 64.43% and 75.80% in the axial and radial directions, respectively. The mean square values of the vibration acceleration were reduced by 67.30% and 91.65% in the axial and radial directions, respectively. This indicated that the radial vibration reduction effect of the spindle rotor was more significant than the axial vibration reduction effect.

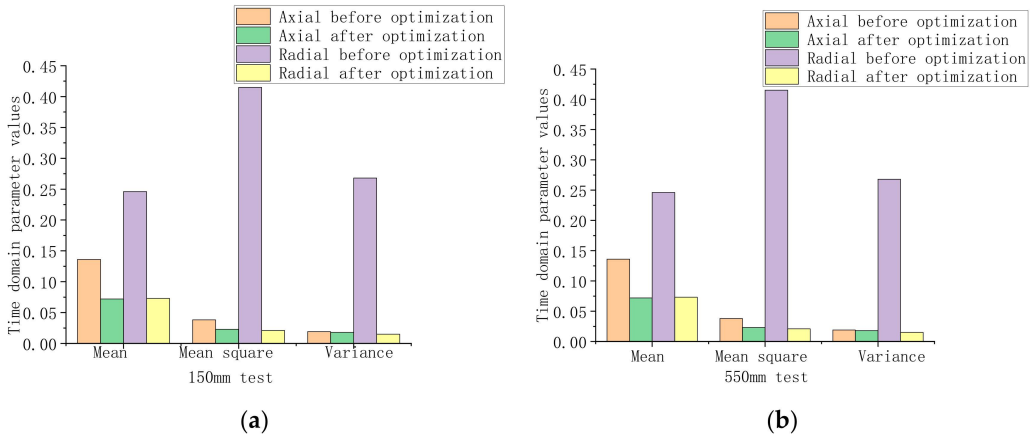

Figure 14. Comparison of shock and vibration test results before and after spindle rotor reduction optimisation: (**a**) 150 mm test; (**b**) 550 mm test.

The difference diagram of the mean, mean square value, variance, and maximum value of the time domain data of the no-load vibration signal before and after the vibration reduction optimisation of the stalk rubbing machine was obtained, which is shown in Figure 15. When the spindle speed changed, by analysing the difference among the five indicators of the time domain data before and after the vibration reduction optimisation of the stalk rubbing machine, the mean value, mean square value, variance, and maximum value of each measuring point in the axial, radial, and plumb directions of the bearing after vibration reduction optimisation were reduced. This indicated that the static component, average energy, fluctuation degree, and peak value of each measuring point vibration were weakened. The change degree of the static component of the vibration of each measuring point was analysed to explore the vibration reduction effect of the stalk rubbing machine. After vibration reduction optimisation, the vibrations of the bearing axial, radial, and plumb directions of the stalk rubbing machine were improved by 5.78%, 10.32%, and 23.96%, respectively. The vibrations of the bearing in the axial, radial, and plumb directions were improved when the spindle speed changed.

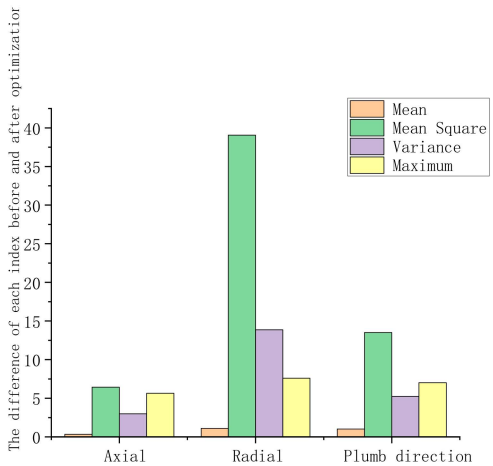

Figure 15. Comparison of time domain data difference in all directions of bearing before and after vibration reduction optimisation.

5. Conclusions

By analysing the simulation test results, we found that the vibration of the rubbing machine rotor excited by the falling collision of small steel balls was attenuated vibration. Therefore, the vibration reduction design was considered by optimising the machine rotor with aluminium foam material to increase its damping. According to the comparative test of simulated stalk impact, the vibration absorption and vibration reduction effect of aluminium foam material on the rubbing machine rotor were as follows: (1) The optimised rotor had a significantly increased damping, and the maximum impact accelerations were reduced by 28.4% and 64.75% in the axial and radial directions within 2 s, respectively. (2) The impact energies decreased by 67.3% and 90.65% in the axial and radial directions within 2 s, respectively. The change degree of the static component of the vibration of each measuring point in the vibration test of the rubbing machine was analysed to explore the vibration reduction effect of the entire machine. After vibration reduction optimisation, the axial, radial, and vertical vibrations of the bearing of the stalk rubbing machine were improved by 5.78%, 10.32%, and 23.96%, respectively. This shows that the vibration of the bearing in three directions was improved when the spindle speed changed. Compared with the vibration reduction of other rotating agricultural machinery, the vibration reduction method mentioned in this study is simple and feasible. It does not need to carry out vibration reduction design for each structure, but only needs to process the foam aluminium material of the machine rotor, which is simple and convenient. Finally, combined with theoretical analysis, simulation tests, and vibration tests, it can be concluded that aluminium foam material has certain vibration reduction and vibration absorption effects in agricultural machinery with impact force, providing new ideas and methods for the research on vibration and noise reduction in agricultural machinery.

Author Contributions: Conceptualisation, Y.Y. and H.T.; methodology, Y.Y. and H.T.; software, D.L. and X.W.; validation, F.L. and X.R.; formal analysis, H.T., F.L., and Y.Y.; investigation, K.Z. and D.L.; resources, H.T.; data curation, F.L., X.W. and X.R.; writing—original draft preparation, Y.Y. and K.Z.; writing—review and editing, Y.Y.; supervision, Y.Y.; project administration, Y.Y. and H.T. All authors have read and agreed to the published version of the manuscript.

Funding: This research was funded by the National Natural Science Foundation of China (Grant No. 32071893), the Science and Technology Program Project of Inner Mongolia Autonomous Region (Grant No. 2022YFDZ0024), the National Natural Science Foundation of China (Grant No. 51765055), and the Inner Mongolia Graduate Student Scientific Innovation Project (Grant No. B20210189Z).

Data Availability Statement: Not applicable.

Acknowledgments: The authors would like to thank the National Natural Science Foundation of China (Grant No. 32071893), the Science and Technology Program Project of Inner Mongolia Autonomous Region (Grant No. 2022YFDZ0024), the National Natural Science Foundation of China (Grant No. 51765055), and the Inner Mongolia Graduate Student Scientific Innovation Project (Grant No. B20210189Z) for financially supporting this research.

Conflicts of Interest: The authors declare no conflict of interest.

References

1. Xiao, M.; Zhang, H.; Zhou, S.; Wang, K.; Ling, C. Research progress and trend of agricultural machinery fault diagnosis technology. *J. Nanjing Agric. Univ.* **2020**, *43*, 979–987.
2. Solecki, L. Preliminary recognition of whole body vibration risk in private farmers working environment. *Ann. Agric. Environ. Med.* **2007**, *6*, 299–304.
3. Chu, T.; Yang, Z.; Han, L. Analysis on satisfied degree and advantage degree of agricultural crop straw feed utilization in China. *Trans. Chin. Soc. Agric. Eng.* **2016**, *32*, 1–9.
4. Chen, C.; Yang, Y.; Xie, G. Study of the development of crop straw management policy in China. *J. China Agric. Univ.* **2016**, *21*, 1–11.
5. Yang, L.; Gao, Y. Bottlenecks of efficient utilization of corn straw feed and its solutions. *J. Jilin Agric. Univ.* **2016**, *38*, 634–638+644.
6. Wang, J.; Xu, C.; Xu, Y.; Wang, J.; Zhou, W.; Wang, Q.; Tang, H. Resonance analysis and vibration reduction optimization of agricultural machinery frame—Taking vegetable precision seeder as an example. *Processes* **2021**, *9*, 1979. [CrossRef]

7. Ji, J.; Chen, K.; Jin, X.; Wang, Z.; Dai, B.; Fan, J.; Lin, X. High-efficiency modal analysis and deformation prediction of rice transplanter based on effective independent method. *Comput. Electron. Agric.* **2020**, *168*, 105126.
8. Son, G.; Kim, B.; Cho, S.; Park, Y. Optimization of the housing shape design for radiated noise reduction of an agricultural electric vehicle gearbox. *Appl. Sci.* **2020**, *10*, 8414. [CrossRef]
9. Wang, J. *Study on Noise Analysis of Rubbing and Breaking Machine*; Inner Mongolia Agricultural University: Hohhot, China, 2010.
10. Wang, J.; Wang, C.; Han, X.; Zhai, Z. The noise research of 9R-40 rub and breaking machine. *J. Agric. Mech. Res.* **2010**, *32*, 212–214+218.
11. Wang, J.; Wang, C.; Wang, F. Numerical simulation on three-dimensional turbulence air flow of 9R-40 rubbing and breaking machine based on fluent software. *Trans. Chin. Soc. Agric. Eng.* **2010**, *26*, 165–169.
12. Zhai, Z.; Zhang, L.; Liu, C.; Li, H.; Cui, H. Numerical simulation and experimental validation of radiation noise from vibrating shell of stalk impeller blower. *Trans. Chin. Soc. Agric. Eng.* **2017**, *33*, 72–79.
13. Zhai, Z.; Wang, C. Numerical simulation and optimization for air flow in impeller blower. *Trans. Chin. Soc. Agric. Mach.* **2008**, *39*, 84–87.
14. Zhai, Z.; Li, H.; Zhao, Y.; Liang, H. Analysis of stress-strain and structure optimization for impeller blower of the stalk rubbing machine. *Mach. Des. Manuf.* **2017**, *07*, 37–40.
15. Zhai, Z.; Zhao, Y.; Wang, L. Stress-strain analysis of throwing impeller based on ABAQUS. *Mach. Des. Manuf.* **2015**, *10*, 42–45.
16. Zhai, Z.; Zhou, L.; Yang, Z.; Zhao, Y.; Gan, S. Analysis on vibration characteristics of throwing impeller of stalk impeller blower. *Trans. Chin. Soc. Agric. Eng.* **2015**, *31*, 17–25.
17. Wang, J.; Dong, H.; Zhai, Z.; Cheng, H.; Kang, X.; Wu, Y. Modal analysis and structure optimization of the rotors of forage rubbing and breaking machine. *Noise Vib. Control* **2018**, *38*, 52–56+61.
18. Lan, Z.; Zhang, L.; Zhai, Z.; Li, Z.; Li, C. Analysis of the influences of structure parameters on pneumatic noise of the impeller blower of the stalk rubbing machine. *J. Agric. Mech. Res.* **2020**, *42*, 34–38+63.
19. Kováčik, J.; Nosko, M.; Mináriková, N.; Simančík, F.; Jerz, J. Closed-cell powder metallurgical aluminium foams reinforced with 3 vol.% sic and 3 vol.% graphite. *Processes* **2021**, *9*, 2031. [CrossRef]
20. Fiedler, T.; Sulong, M.A.; Mathier, V.; Belova, I.V.; Younger, C.; Murch, G.E. Mechanical properties of aluminium foam derived from infiltration casting of salt dough. *Comput. Mater. Sci.* **2014**, *81*, 246–248. [CrossRef]
21. Belardi, V.G.; Fanelli, P.; Trupiano, S.; Vivio, F. Multiscale analysis and mechanical characterization of open-cell foams by simplified FE modeling. *Eur. J. Mech. A: Solids* **2021**, *89*, 104291. [CrossRef]
22. Norbert, O.; Attila, S.; Alexandra, K.; Domonkos, K. Compressive mechanical properties of low-cost, aluminium matrix syntactic foams. *Compos. Part A Appl. Sci. Manuf.* **2020**, *135*, 105923.
23. Su, L.; Liu, H.; Yao, G.; Zhang, J. Experimental study on the closed-cell aluminum foam shock absorption layer of a high-speed railway tunnel. *Soil Dyn. Earthq. Eng.* **2019**, *119*, 331–345. [CrossRef]
24. Rajak, D.; Mahajan, N.; Selvaraj, S.K. Fabrication and experimental investigation on deformation behaviour of $AlSi_{10}Mg$ foam-filled mild steel tubes. *Trans. Indian Inst. Met.* **2020**, *73*, 587–594. [CrossRef]
25. Fomin, O.; Lovska, A.F.; Skok, P.O.; Rybin, A.V. Feasibility study for using the fillers in the bearing structure components of a gondola car. *Nauk. Visnyk Natsionalnoho Hirnychoho Universytetu* **2022**, *1*, 51–56. [CrossRef]
26. Lu, X.; Sun, W.; Liang, J.; Xie, J.; Lu, Z. Experimental research on exhaust silencer of foamed aluminum alloy. *Trans. Chin. Soc. Agric. Mach.* **1999**, *5*, 36–40.
27. Ashby, M.F.; Evans, A.; Fleck, N.A.; Gibson, L.J.; Hutchinson, J.W.; Wadley, H.N.G. Metal foams: A design guide: Butterworth-Heinemann. *Mater. Des.* **2002**, *23*, 119. [CrossRef]
28. Crupi, V.; Epasto, G.; Guglielmino, E. Impact response of aluminum foam sandwiches for light-weight ship structures. *Metals* **2011**, *1*, 98–112. [CrossRef]
29. Banhart, J. Light-metal foams-history of innovation and technological challenges. *Adv. Eng. Mater.* **2013**, *15*, 82–111. [CrossRef]
30. Jia, R.; Zhao, G. Progress in constitutive behavior of aluminum foam. *Chin. J. Theor. Appl. Mech.* **2020**, *52*, 603–622.
31. Wan, T.; Liu, Y.; Zhou, C.; Chen, X.; Li, Y. Fabrication, properties, and applications of open-cell aluminum foams: A review. *J. Mater. Sci. Technol.* **2021**, *62*, 11–24. [CrossRef]
32. Albertelli, P.; Esposito, S.; Valerio, M.; Massimo, G.; Michele, M. Effect of metal foam on vibration damping and its modelling. *Int. J. Adv. Manuf. Technol.* **2021**, *117*, 2349–2358. [CrossRef]
33. Wang, J.; Xu, H.; Ma, N. Investigation on simulation and response of impact between flexible cantilever and steel ball. *Chin. J. Appl. Mech.* **2010**, *27*, 471–475+638.
34. Bapat, C.; Popplewell, N. Several similar vibroimpact systems. *J. Sound Vib.* **1987**, *113*, 17–28. [CrossRef]
35. Qin, Z.; Lu, Q. Analysis of process model based on restitution coefficient. *J. Dyn. Control* **2006**, *12*, 294–297.
36. Zhu, D.; Xing, Y. Analytical solution of point elastic impact between structures. *Chin. J. Theor. Appl. Mech.* **1996**, *28*, 99–103.
37. Yousuf, L.S. Influence of nonlinear dynamics behavior of the roller follower on the contact stress of polydyne cam profile. *Processes* **2022**, *10*, 585. [CrossRef]
38. Li, W.; Chen, T.; Hu, X.; Huang, X. Computer simulation of vibroimpact absorbers. *J. Xi'an Jiaotong Univ.* **1998**, *32*, 32–35.
39. Xing, Y. Analytical solution of linear elastic collision of beam structure. *J. Beijing Univ. Aeronaut. Astronaut.* **1998**, *24*, 633–637.
40. Li, F. *Experiment and Simulation Study of Sub-Impact in Beam Struck by Sphere*; Anhui University of Technology: Hefei, China, 2016.

41. Qi, X.; Yin, X.; Yang, H.; Jin, T. Study of sub-impact in simply supported beam struck by steel sphere. *J. Mech. Strength* **2015**, *37*, 45–51.
42. Wang, P.; Li, G.; Li, X. Vibration characteristics analysis of o-shaped damping ring to balance damping gear transmission system for three-cylinder engine. *Processes* **2022**, *10*, 1685. [CrossRef]

Disclaimer/Publisher's Note: The statements, opinions and data contained in all publications are solely those of the individual author(s) and contributor(s) and not of MDPI and/or the editor(s). MDPI and/or the editor(s) disclaim responsibility for any injury to people or property resulting from any ideas, methods, instructions or products referred to in the content.